Cancer Research

Spatially Resolved Metabolic Phenotyping of Breast Cancer by Desorption Electrospray Ionization Mass Spectrometry

Sabine Guenther[1], Laura J. Muirhead[2], Abigail V.M. Speller[1], Ottmar Golf[1], Nicole Strittmatter[1], Rathi Ramakrishnan[3], Robert D. Goldin[3], Emrys Jones[1], Kirill Veselkov[1], Jeremy Nicholson[1], Ara Darzi[2], and Zoltan Takats[1]

Abstract

Breast cancer is a heterogeneous disease characterized by varying responses to therapeutic agents and significant differences in long-term survival. Thus, there remains an unmet need for early diagnostic and prognostic tools and improved histologic characterization for more accurate disease stratification and personalized therapeutic intervention. This study evaluated a comprehensive metabolic phenotyping method in breast cancer tissue that uses desorption electrospray ionization mass spectrometry imaging (DESI MSI), both as a novel diagnostic tool and as a method to further characterize metabolic changes in breast cancer tissue and the tumor microenvironment. In this prospective single-center study, 126 intraoperative tissue biopsies from tumor and tumor bed from 50 patients undergoing surgical resections were subject to DESI MSI. Global DESI MSI models were able to distinguish adipose, stromal, and glandular tissue based on their metabolomic fingerprint. Tumor tissue and tumor-associated stroma showed evident changes in their fatty acid and phospholipid composition compared with normal glandular and stromal tissue. Diagnosis of breast cancer was achieved with an accuracy of 98.2% based on DESI MSI data (PPV 0.96, NVP 1, specificity 0.96, sensitivity 1). In the tumor group, correlation between metabolomic profile and tumor grade/hormone receptor status was found. Overall classification accuracy was 87.7% (PPV 0.92, NPV 0.9, specificity 0.9, sensitivity 0.92). These results demonstrate that DESI MSI may be a valuable tool in the improved diagnosis of breast cancer in the future. The identified tumor-associated metabolic changes support theories of *de novo* lipogenesis in tumor tissue and the role of stroma tissue in tumor growth and development and overall disease prognosis. *Cancer Res; 75(9); 1828–37. ©2015 AACR.*

Downloaded from http://aacrjournals.org/cancerres/article-pdf/75/9/1828/2729351/1828.pdf by guest on 21 February 2024

Introduction

Breast cancer is the most common cancer in women; approximately 12.3% of women in the United States will be diagnosed with breast cancer at some point in their lifetime. It is a heterogeneous disease with disparate patient outcomes dependant on multiple factors, including tumor size, nodal status, histologic grade and type, peritumoral vascular invasion, HER2, and hormone receptor (HR) status. A proportion of breast cancers will benefit from systemic chemotherapy, endocrine, and HER2-based therapies. HR and HER2 receptor expression are strongly predictive biomarkers for the response to targeted therapies. Results of these tests alone are key determinants of which adjuvant treatment the patient receives. There is, however, evidence of variability in assay results with discordance between laboratories, as there is no gold standard immunohistochemical assay available (1). Furthermore, these traditional pathologic prognostic categories are currently not sufficient to fully elucidate which patients will see the greatest benefit from these treatments. As such, further research into improving the management of breast cancer by early diagnosis, accurate characterization of disease, focused, personalized treatment, and risk stratification is essential. Significant progress has been made in the development of tissue-based tests that aim to predict risk of recurrence in patients with early-stage breast cancer and ductal carcinoma *in situ*. These include gene expression profiling assays such as Oncotype Dx (2), MammaPrint (3), PAM50 (4), and expanded immunohistochemistry tests such as IHC4 (5), and Mammostrat (6).

Both genetic/epigenetic (7–9) and metabolic (10) changes have been demonstrated in the histologically normal tissue surrounding invasive breast cancer compared with distant tissue, or that which has been excised for completely benign disease. These changes support the still incompletely understood theory of field cancerization. There is growing evidence that peritumoral microenvironmental changes may represent underlying mechanisms that affect tumor cell initiation, progression, and disease prognosis (11) and may affect surgical

[1]Section of Computational and Systems Medicine, Department of Surgery and Cancer, Faculty of Medicine, Imperial College London, London, United Kingdom. [2]Section of Biosurgery and Surgical Technology, Department of Surgery and Cancer, Faculty of Medicine, Imperial College London, London, United Kingdom. [3]Centre for Pathology, Department of Medicine, Imperial College London, London, United Kingdom.

Note: Supplementary data for this article are available at Cancer Research Online (http://cancerres.aacrjournals.org/).

Corresponding Author: Zoltan Takats, Department of Surgery and Cancer, Faculty of Medicine, Imperial College London, 371 SAF Building, South Kensington Campus, London SW7 2AZ, United Kingdom. Phone: 44-20-7594-2760; Fax: 44-20-7594-3226; E-mail: z.takats@imperial.ac.uk

doi: 10.1158/0008-5472.CAN-14-2258

©2015 American Association for Cancer Research.

margins and risk of recurrence. Dynamic contrast enhanced magnetic resonance imaging has been used to identify this tumor-associated stroma (12).

Over the last decade, mass spectrometry imaging (MSI) has been increasingly applied to investigate the spatial distribution of biomolecules in tissue sections (13–15). Its potential to reveal the distribution of hundreds of molecules in a single measurement, without prior derivatization, is especially useful for the clinicopathologic analysis of cancer (16–18). Desorption electrospray ionization (DESI) MSI allows the detection of small metabolites and complex lipids within a tissue sample (19, 20). DESI MSI is not *per se* a quantitative method, but allows for relative quantification when the same tissue type is compared. It may be applied to fresh or frozen tissue sections without the need for further sample preparation, and as such may be readily incorporated into the operating theater and/or histopathologic workflow as recently demonstrated for the intraoperative determination of margin status in brain tumor surgery (21–23).

This study applied DESI MSI to the analysis of breast cancer to determine whether this technique can provide further information on the metabolic changes in breast tumor tissue and peritumoral tissue, which may provide novel biomarkers for stratification and prognostication of the disease and improve our understanding of tumor/microenvironment metabolomics and field cancerization. Moreover, we investigate the association between the metabolomic profile of the tissue and clinical factors such as cancer type, grade, and HR status.

Materials and Methods

Clinical study and patient recruitment

This was a single center, prospective observational study performed at Charing Cross Hospital (London, United Kingdom; REC 11/LO/0686). Female patients undergoing breast surgery for benign and malignant disease were recruited on the day of surgery, having previously agreed to contribute tissue to this study, which was approved by the local Ethical Review Board. Patients who had undergone neoadjuvant therapy were included, and this was documented in the corresponding clinical dataset, as was medical history, drug history, menopausal state, ethnicity, smoking, alcohol status, and lifetime use of HR such as the oral contraceptive pill or hormone replacement therapy. Intraoperative biopsies were taken from the lesion (28 patients, 28 samples) and tumor bed (22 patients, 98 samples), flash frozen, and stored at −80°C. The "tumor bed" in this context is used to describe healthy tissue in the cavity beyond the surgical resection margin. Tissue was sampled intraoperatively using a disposable core biopsy gun (TruCore II 14G × 10 cm). One biopsy sample was taken from each tumor and 4 to 5 biopsy samples were taken from the tumor bed; at 3, 6, 9, and 12 o'clock and, from the posterior/deep cavity wall where possible. Demographic and clinicopathologic characteristics of the patient cohort are summarized in Table 1.

Table 1. Demographic and clinicopathologic characteristics

	Patients, *n*	Samples	%	Median age (range)
Tumor bed biopsies	22	98	44	55 (17–87)
Tumor biopsies	28	28	56	61 (44–90)
Tumor type				
IDC	19		68	63 (44–90)
Invasive lobular carcinoma (ILC)	9		32	59 (48–86)
Tumor grade				
T1	2		7	61 (53–69)
T2	13		46	62 (44–87)
T3	13		46	59 (45–90)
HR status[a]				
Negative	12		43	61 (45–90)
Positive	15		54	59 (44–87)
HER2 receptor status[a]				
Negative	20		71	57 (44–87)
Positive	7		25	64 (51–90)
Lymph node status[a]				
Negative	13		29	59 (44–85)
Positive	13		61	62 (45–90)

[a]Information about HR, HER2 receptor, and lymph node status was not available for one patient. Lymph node status was also not available for another patient.

Sample preparation and mass spectrometry analysis

Frozen tissue sections (thickness, 15 μm) were prepared from each sample and subjected to DESI MSI. After measurement, tissue sections were hematoxylin and eosin (H&E) stained and underwent histologic examination. For DESI analysis, tissue sections were brought to room temperature. DESI MSI was carried out using a home-built DESI ion source coupled to a high-resolution orbital trapping mass spectrometer (Exactive, Thermo Scientifc GmbH). The DESI ion source was operated at a spatial resolution of 100 μm using nitrogen pressure of 4 bar, high voltage of 4.5 kV, a solvent mixture of methanol and water in a ratio 95:5 and a flow rate of 1.5 μL/minute. The mass analysis was carried out in negative ion mode in the mass range $m/z = 200$–1,000 at a nominal mass resolution of 100,000 at $m/z = 200$ and a mass accuracy of ± 2 ppm.

Statistical analysis

Raw mass spectrometric data were converted to imzML format (24) via imzML Converter (version 1.0.5) and imported into MATLAB (R2013a) for preprocessing (described in the Supplementary Material and Methods) and analysis. Preprocessed data were subjected to multivariate statistical data analysis. Recursive maximum margin criterion (RMMC) analysis was used for supervised discrimination and classification (25, 26). Tissue types in each sample and their spatial distribution were determined by histologic examination by an independent consultant histopathologist. This information was then used to select a small number of representative mass spectra per tissue type from the MSI image to build a sample-specific RMMC model and to classify all pixels of the MSI image via this model. One hundred of the correctly classified mass spectra were randomly selected and used to calculate an averaged mass spectrum for the tissue types present in the sample. If several tumor bed samples were measured per patient, average spectra for the tissue types present in the samples were calculated. After this step, each patient was represented by a set of average mass spectra corresponding to each tissue type found in the samples taken from this patient. This reduced dataset was then subjected to RMMC analysis to answer global questions regarding the differentiation of tissue types, tumor, and nontumor tissue, cancer type, cancer grade, and receptor status. Numbers of patients and samples per group of the reported models are given in Supplementary Table S1. The histopathologic data were retrieved from patient records and were used for data grouping in the corresponding models. Discriminating models were validated using 10-fold cross validation

Downloaded from http://aacrjournals.org/cancerres/article-pdf/75/9/1828/2729351/1828.pdf by guest on 21 February 2024

(described in Supplementary Materials and Methods). Confusion matrices were used to show the accuracy of a classification result. In case of two classes, the receiver operating characteristic (ROC) curve and corresponding area under the curve (AUC) were further employed for discriminative model diagnostics. The contributions of *m*/*z* features into multivariate models (component weights) were used for ranking of discriminant-related features. In addition, the univariate ANOVA analysis was employed to identify discriminatory *m*/*z* variables. The derived *P* values were adjusted with the false discovery rate of 0.003 for the tumor/tumor bed model, 0.005 for the tumor/glandular tissue model, and 0.01 for the stroma/tumor stroma and grade/HR model. After identification of class separating *m*/*z* bins via contributions plots and based on *P* values, exact *m*/*z* values were retrieved from the raw data. These values and isotopic patterns were used for compound identification via database search [Metlin (27), Lipid maps (28), HMDB (29)].

Results

Cancer diagnostics

We first determined the ability of DESI MSI to identify the presence of breast cancer based on its global metabolic profile from 126 tissue biopsy samples derived from 50 patients. Data extracted from DESI MSI measurements were separated in two groups (tumor from 28 patients and tumor bed from 22 patients) and subjected to multivariate statistical analysis. Tumor bed samples were used as the normal control and were confirmed as morphologically normal tissue by histologic examination. RMMC analysis demonstrated significant class separation in the cross-validated score plot (Fig. 1A). The predictive power of the model was good, with 98.2% of data points correctly classified as tumor and tumor bed (Fig. 1B). One tumor sample was incorrectly classified as histologically normal tissue by the model (highlighted by an additional circle in green in Fig. 1A). Figure 1C shows the raw summary mass

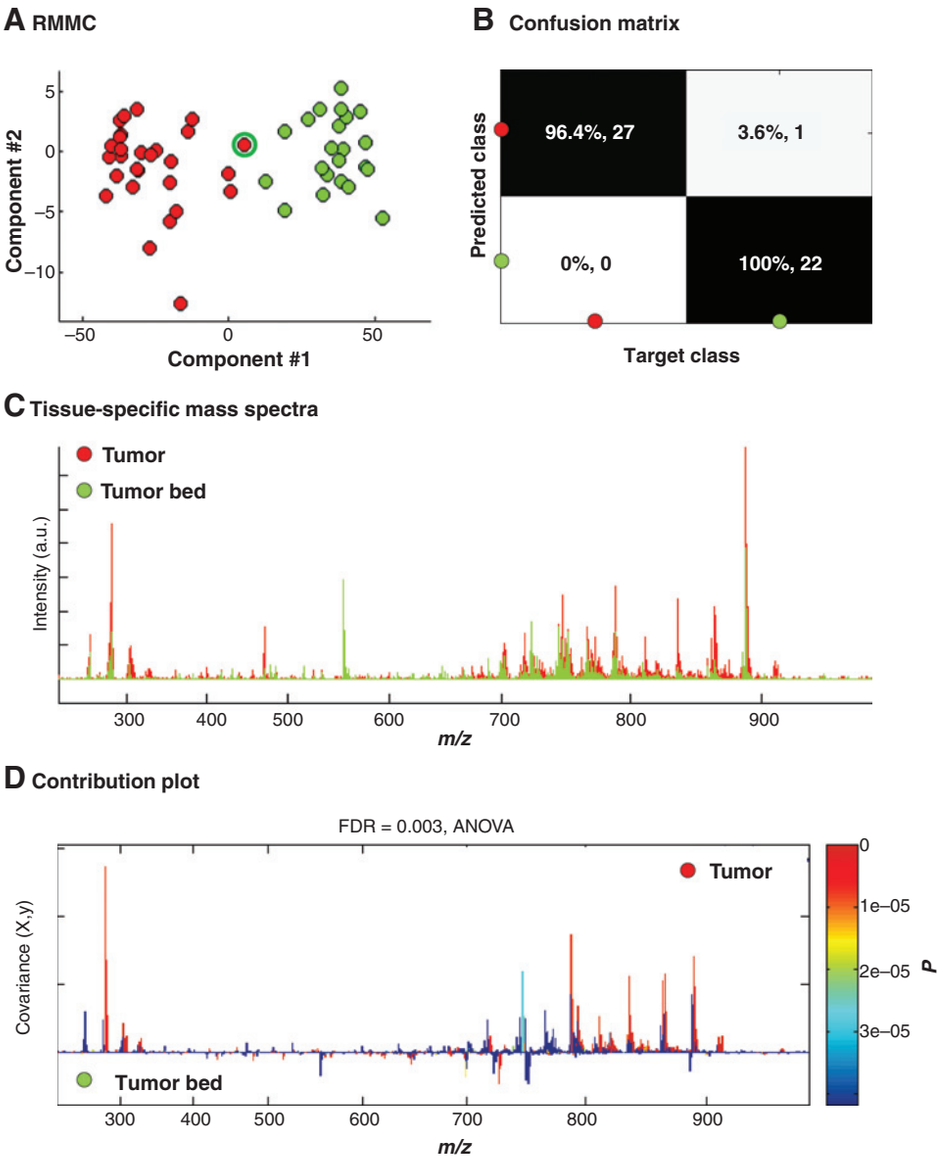

Figure 1.
Differentiation of tumor (red) and tumor bed samples (green) based on metabolomic profiles measured with DESI MSI. A, 10-fold cross-validated RMMC score plot (each patient is maximally represented by one point in each group; for each point maximum, 100 randomly selected spectra were averaged) showing the separation of the two groups using multivariate analysis. B, confusion matrix showing classification results based on mahalanobis distance (98.2% overall correct assignment). C, representation of the tissue-specific metabolomic profiles. D, contribution plot showing the contribution of each signal in the metabolomic profiles to the group separation by a color bar (lower *P* values indicate higher significance for group separation). False discovery rate (FDR) was 0.003 or <1 sample for signals in red color.

Downloaded from http://aacrjournals.org/cancerres/article-pdf/75/9/1828/2729351/1828.pdf by guest on 21 February 2024

Table 2. Compounds found most discriminating between morphologically normal glandular tissue and tumor tissue (FDR: 0.005)

Compound	Ion	*m/z* value	Mean intensity tumor	Mean intensity glandular tissue	Fold change	*P*
FA(16:1)	M−H	253.22	149	37	4	1.9×10^{-5}
FA(18:1)	M−H	281.25	2,361	648	4	7.5×10^{-6}
FA(20:3)	M−H	305.25	281	41	7	1.8×10^{-7}
FA(20:2)	M−H	307.27	131	13	10	4.1×10^{-7}
FA(20:1)	M−H	309.29	181	22	8	9.3×10^{-7}
FA(22:5)	M−H	329.25	114	37	3	3.4×10^{-5}
FA(22:4)	M−H	331.27	149	36	4	1.8×10^{-6}
FA(24:1)	M−H	365.35	57	4	14	1.3×10^{-5}
LPI(18:1)	M−H	599.33	79	13	6	1.3×10^{-5}
PE(32:0)	M−H	690.51	52	11	5	1.3×10^{-5}
PE(35:1)	M−H	730.55	79	13	6	1.3×10^{-5}
PC(34:2)	M+Cl	792.54	264	125	2	4.6×10^{-5}
PC(34:1)	M+Cl	794.55	519	166	3	4.6×10^{-7}
PS(38:3)	M−H	812.55	428	199	2	2.3×10^{-5}
PC(36:1)	M+Cl	822.59	122	33	4	4.9×10^{-6}
PI(36:3)	M−H	859.54	377	127	3	4.6×10^{-5}
PI(38:3)	M−H	887.57	1,213	370	3	1.6×10^{-5}
PI(40:5)	M−H	911.57	177	76	2	3.5×10^{-5}
PI(40:4)	M−H	913.59	182	53	3	8.3×10^{-5}

spectrometric profiles of the two groups (tumor and tumor bed). Both tissue profiles feature a high number of peaks (3,500 were used to build the model), especially in the mass range of fatty acids (m/z = 200–400) and phospholipids (m/z = 650–950). Although the majority of features were found in both tissue profiles, the abundance of the individual features differed for the two groups. The contribution plot shown in Fig. 1D indicates that fatty acids in general and phospholipids with a mass greater than 760 Da are more abundant in tumor tissue, while a small number of features in the mass range 700–760 Da are significantly higher in the morphologically normal breast tissue. Free fatty acid and phospholipid markers that have a high contribution to the class separation are summarized in Table 2 and will be described in detail in the discussion section.

Tissue-specific metabolomic profiling

The main advantage of DESI MSI is that it allows spatially resolved profiling of tissue sections. This requires sophisticated statistical analysis, but allows biochemical changes, for example due to cancer initiation and histologic variation, to be visualized and objectively analyzed. Breast tissue is microscopically composed of adipose tissue (approximately 60%), glandular tissue (approximately 30%), and stroma. These were the main tissue components identified during histologic evaluation of samples in this study. Accordingly, mass spectrometric profiles for each of these tissue subclasses were extracted per sample and patient. Within our study, we examined conventional "breast cancer," that is, cases of malignancy in which the neoplastic cells demonstrates an epithelial (glandular) phenotype.

Tumors, in the macroscopic sense, contain multiple tissue types in addition to tumor cells; often in the form of stroma and rarely as adipose tissue. For the purpose of analysis, histologically normal stroma and adipose tissue directly associated with malignant cells (macroscopically intratumoral) was extracted separately from this same tissue type located within the tumor bed. Some samples featured blood vessels and nerves with diameters of >100 μm. Because of the low number of samples these were excluded from statistical data analysis. Figure 2A shows the cross-validated RMMC scores plot for the tissue type–specific analysis of the dataset, differentiating six tissue subclasses: adipose tissue from tumor bed, stroma from tumor bed, glandular tissue from tumor bed, tumor-associated stroma, tumor-associated adipose tissue, and tumor itself (neoplastic glandular cells). There was 83.8% overall correct classification (Fig. 2B), and despite significant metabolic homogeneity in these tissue type subclasses, only a single tumor sample (the same as in the previous model) was incorrectly classified. This demonstrates that tumor tissue has a distinctly different metabolomic profile in comparison with benign tissues. Of particular note is that tumor demonstrates a different profile to benign glandular tissue. Interestingly tumor-associated stroma was also found to clearly separate from tumor bed stroma. This highlights the fact that stromal tissue within the tumor microenvironment also undergoes a detectable metabolic change. The most significant mass spectrometric differences were observed between stromal tissue and all other tissue types, most likely due to the low abundance of phospholipids in collagen-rich tissue.

The observed differences in metabolomic tissue profiles were sufficient for the classification of unknown tissue types using multivariate statistical methods. Figure 2C shows the results for biopsies taken from two patients. It compares the H&E–stained tissue section (stained after DESI MSI measurement) with a tissue map that was reconstructed after classification of each pixel of the DESI MSI measurements using multivariate statistical analysis. For purposes of classification, a model was built based on the metabolomic tissue profiles extracted from all samples leaving out the data of the sample to be classified. The probability of a pixel to belong to a specific tissue type within the model is visualized by intensity of the color representative of that tissue type. Further details of model generation and classification can be found in the Supplementary Material. On the left of the figure, an H&E–stained tumor bed biopsy with histologically normal stromal, glandular, and adipose tissue and the associated DESI MSI tissue map is shown. On the right, an H&E–stained tissue section of grade 3, HR negative, invasive ductal carcinoma (IDC; with necrosis and a large amount of tumor invading stroma in the superior aspect of the tissue section, and histologically normal stroma and adipose tissue in

Downloaded from http://aacrjournals.org/cancerres/article-pdf/75/9/1828/2729351/1828.pdf by guest on 21 February 2024

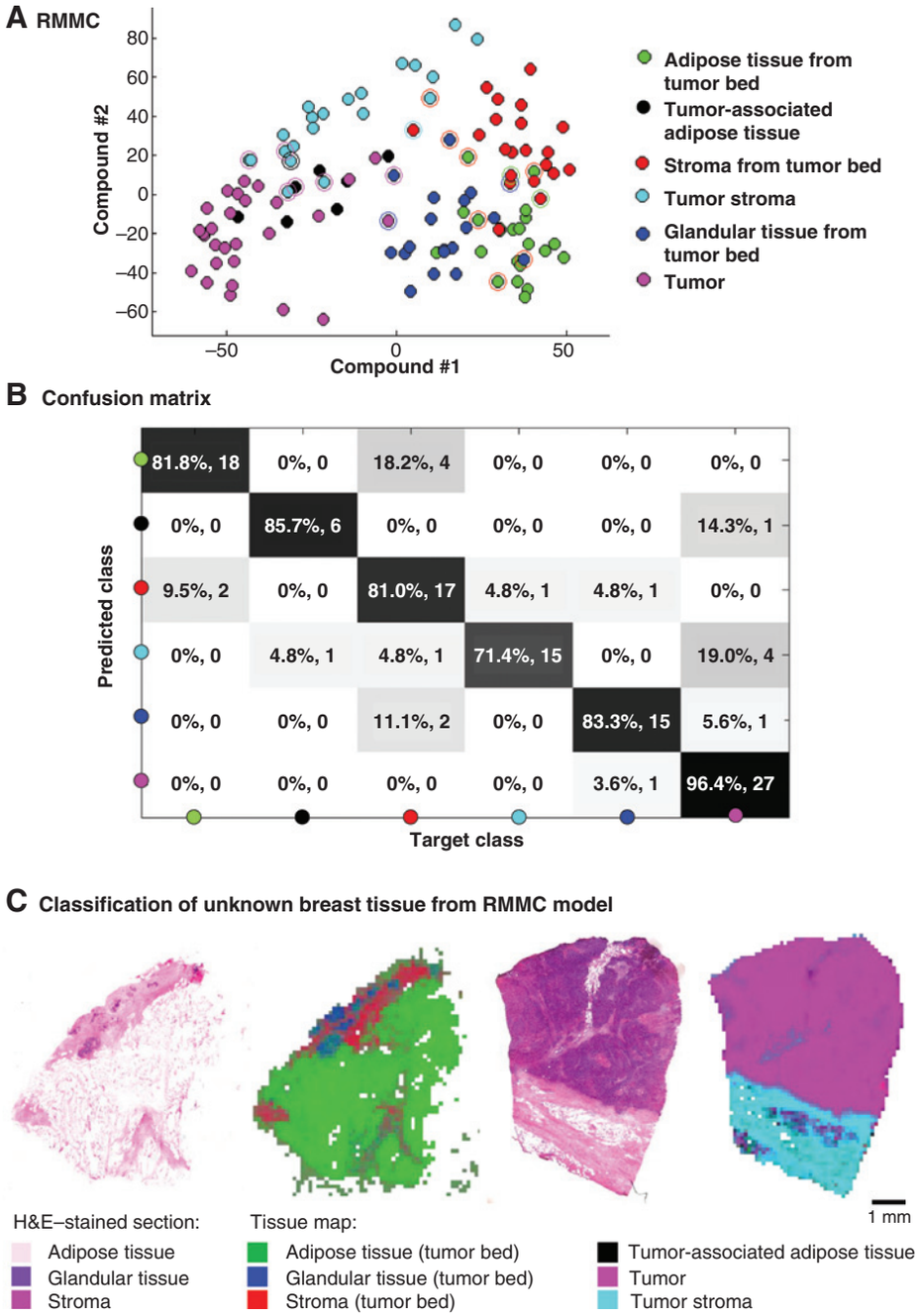

Figure 2.
Differentiation of tissues present in tumor and tumor bed samples based on the metabolomic profiles measured with DESI MSI. A, 10-fold cross-validated RMMC score plot (each patient is maximally represented by one point in each group; for each point maximum, 100 randomly selected spectra were averaged) showing the separation of the groups using multivariate analysis. B, confusion matrix showing classification results based on mahalanobis distance (83.8% overall correct assignment). C, comparison of H&E–stained tissue section (stained after DESI MSI) used for histologic evaluation and tissue classification results from multivariate statistical analysis of the DESI MSI metabolomic data. Colored pixels correspond to tissues as indicated in the Figure legend. Left, a tumor bed biopsy. Right, a grade 3 IDC with negative HR status.

the inferior aspect). The associated DESI MSI tissue map is adjacent. Tissue types, as identified in the H&E–stained section, were also accurately classified with low lateral resolution by multivariate statistical analysis of the metabolomic data, thus showing the potential of this method for the detection of tumor tissue without histologic staining. The method shown here is proof-of-concept and could be improved by adding more tissue types and samples to the model.

To further investigate the previously described peritumoral metabolomic changes associated with breast cancer, glandular tissue was specifically examined by statistical data analysis. This tissue-specific comparison allows any direct changes in the metabolome of the glandular tissue due to cancer development to be characterized, without interference by the metabolome of adjacent tissue, as often observed in bulk tissue analysis. DESI MSI as performed here is not a quantitative method, but allows for relative quantification when, as shown below, if data from the same tissue type are compared. In this study, mass spectrometric profiles of morphologically normal glandular tissue (18 patients) were compared with those of tumor tissue

Downloaded from http://aacrjournals.org/cancerres/article-pdf/75/9/1828/2729351/1828.pdf by guest on 21 February 2024

Table 3. Compounds most significant in discriminating between morphologically normal stroma of the tumor bed and tumor-associated stroma (FDR: 0.01)

Compound	Ion	*m/z* value	Mean intensity tumor stroma	Mean intensity stroma tumor bed	Fold change	*P*
Lactate	2M+Na	201.04	84	2	37	3.4×10^{-8}
FA(20:3)	M−H	305.25	82	12	7	1.1×10^{-5}
Lactate	$M+Na_4Cl_4$	320.86	35	1	26	1.2×10^{-6}
Calcidiol	M−2H+Na	421.32	36	1	33	5.1×10^{-8}
LPS(20:3)	M−H2O-H	528.28	43	8	5	5.6×10^{-6}
PC(38:4)	M+Cl	844.57	78	14	6	5.0×10^{-6}
PI(36:1)	M−H	863.57	129	38	3	1.6×10^{-5}

(28 patients). The contribution of each signal to the separation of the groups was calculated. The vast majority of peaks were found to be more abundant in the tumor tissue. The most intense peaks (with a P value $<1 \times 10^{-5}$) are summarized in Table 2 with tentative identifications along with mean values and fold change for the morphologically normal glandular breast tissue and tumor tissue. Among the highly significant peaks identified were several fatty acids (FA), phosphatidylethanolamines (PE), phosphatidylcholines (PC) and phosphatidylinositols (PI). Fold changes between 2 and 14 were observed (mean fold change = 5), which is close to fold changes reported in the literature (30, 31). Only a small number of peaks with medium significance for tissue separation were found in greater abundance in the morphologically normal glandular tissue. These signals were identified as the ether lipids p-PE(36:4), p-PE(38:4), p-PE(38:5) and PA(36:1).

To elucidate the metabolomic changes associated with cancer progression and invasion as found in DESI MS spectra in more detail, stroma was examined independently by statistical data analysis. In our study, mass spectrometric profiles of morphologically normal stroma from the tumor bed (20 patients) were compared with stroma directly associated with the tumor (20 patients). Again, there was a greater abundance of signals from fatty acids and lipids in "tumor associated" stroma compared with stroma from histologically normal tissue. The most intense peaks, with a P value $< 2 \times 10^{-5}$, are summarized in Table 3. Very high fold changes (26–37) were found for signals associated with lactate and calcidiol. Lactate was found as a dimer and in form of several sodium chloride clusters ($M+Na_4Cl_4$, $M+Na_3Cl_3$, $M+Na_2Cl_2$). Salt clusters are likely to be observed in stroma, as this tissue serves as a water and salt depot for the surrounding tissues (32). The monomer, however, was not accessible in the given measurement range.

Associations of metabolomic profiles with clinical factors

Finally, the group of tumor samples was divided into subgroups (see Table 1) according to a range of clinical factors employed in the prognostication and management of breast cancer. Among these were the histologic grade and type of tumor, lymph node status, HR [estrogen (ER) and progesterone (PR)] status and HER2 receptor status. Each of these clinical factors was tested individually (independently of all other clinical factors) to fit the metabonomic differences observed in the data of the tumor tissue. Patients were excluded from the dataset when no data for the tested clinical factor were available. Differences in the metabolic data were best explained by tumor grade (Fig. 3) and HR status (Fig. 4) and slightly less accurately by tumor type (see Supplementary Fig. S1).

The correlation of the metabonomic data with the tumor grade is shown in Fig. 3 for tumor grade 3, tumor grade 2, and morphologically normal glandular tissue. The cross-validated RMMC score plot for this dataset is shown in Fig. 3A. The corresponding confusion matrix is given in Fig. 3B. An overall classification accuracy of 88.6% was achieved. The ROC curve shows the potential to use the metabolomic data for the discrimination of grade 2 and grade 3 tumors (Fig. 3C). The probability for correct discrimination was 97% (AUC = 0.97).

The correlation of the metabonomic data with HR status of the tumor tissue is shown in Fig. 4 for tumors with positive HR status, tumors with negative HR status, and morphologically normal glandular tissue. An overall classification accuracy of 86.7% was achieved for this model (Fig. 4A and B). The probability for correct discrimination of HR-positive and HR-negative tumors was 96% (AUC = 0.96, Fig. 4C).

Tumor grade and HR status fitted the metabolomic data with similar quality due to the 86% overlap of the two clinical factors. Hence, a combination of tumor grade and HR was used for further interpretation.

Supplementary Figure S2 shows intensity distribution plots of 8 compounds with P values $< 2 \times 10^{-4}$. Supplementary Figure S3 shows the distribution of FA(20:2) in a tumor bed sample (a), in a grade 2 HR-positive tumor sample (b) and a grade 3 HR-negative tumor sample (c). From a clinical point of view, a separation between grade 2, HR-positive tumors and grade 3, HR-negative tumors is relevant, as the former are generally associated with a better response to adjuvant therapy and a better prognosis, while the opposite is true of the latter (33).

Discussion

Cancer diagnostics

Results correspond well with previous measurements of the metabolic profile of breast cancer. Studies using both using mass spectrometry (30) and NMR spectroscopy (34) have documented an increase in both FA and phospholipid concentrations in breast cancer tissue in comparison with morphologically normal breast tissue. The single misclassified sample in our study showed lower overall intensity in the average spectrum when compared with the other tumor samples. Lower overall intensity might be related to the low density of malignant cells in the tissue section. No clinical (tumor type, tumor grade, ER, PR, HER2, lymph node status, preoperative treatment) or demographic (age, ethnicity, lifestyle) features were found that explain the misclassification.

Alterations in stroma and glandular tissue due to cancerization and immune response

Cancer is generally associated with a loss of differentiation, unregulated growth, and increased cell mobility. Research into the mechanisms involved in the transformation of normal epithelial cells into cancer cells has already determined dramatic changes in the genome (35, 36), proteome (37, 38), and

Downloaded from http://aacrjournals.org/cancerres/article-pdf/75/9/1828/2729351/1828.pdf by guest on 21 February 2024

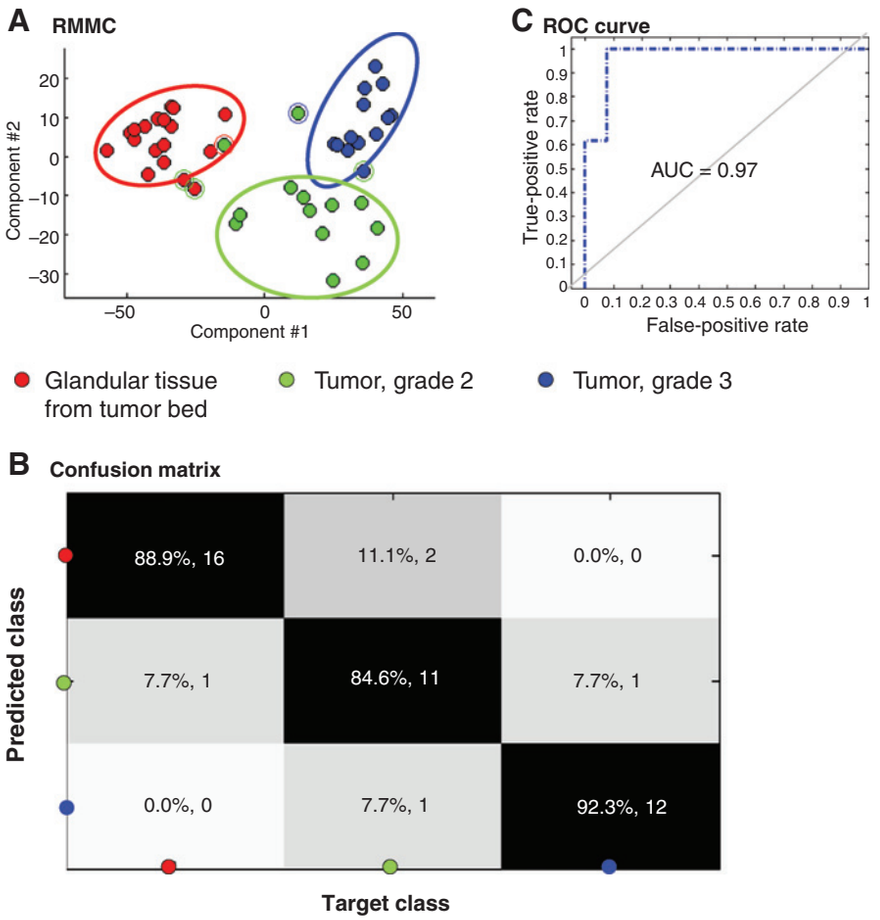

Figure 3.
Association of metabolomic DESI MSI profiles of normal glandular and tumor (ILC and IDC) tissue with tumor grade. A, 10-fold cross-validated RMMC score plot (each patient is maximally represented by one point in each group; for each point maximum, 100 randomly selected spectra were averaged) showing the separation of normal glandular tissue, grade 2 tumors, and grade 3 tumors using multivariate data analysis. B, confusion matrix of the RMMC model showing classification results based on mahalanobis distance (88.6% overall correct assignment). C, ROC curve showing the potential of the model to discriminate between grade 2 tumors and grade 3 tumors.

metabolome (39, 40) of these cells. Among these changes, an alteration in the glucose metabolism (41), in the fatty acid (31, 34) as well as in the lipid composition of the cells (30) has been observed. In particular, fatty acids from *de novo* synthesis were found in greater abundance. These findings were replicated in our dataset where five of the seven fatty acids found to be increased in tumor tissue can be generated via *de novo* synthesis. Higher PC and PE levels have been reported previously in breast cancer (31, 42, 43) and these could be associated with the loss of differentiation and, more specifically, a loss of epithelial polarity. Previous studies have shown that PEs and PCs were upregulated, while p-PEs were downregulated in Madin–Darby canine kidney cells (a cell culture model for epithelial polarization) after the cells underwent epithelial–mesenchymal transition (42).

There are similarities in the immune response toward wounds and toward tumors, such as the activation of extracellular matrix remodeling, cell motility, and angiogenesis (44). Furthermore, there is increasing evidence that the tumor environment plays an active role in tumor development and progression (45). Tumor cells are known to interact with their surrounding tissue and may manipulate the function of cells such as fibroblasts, endothelial cells, and pericytes (46, 47). Fibroblasts are highly abundant in the tumor environment (47). They have been shown to undergo differentiation to cancer-associated fibroblasts (CAF) and to produce lactate and pyruvate through aerobic glycolysis, prompting tumor cells to overcome energy depletion (reverse Warburg effect; ref. 48). However, tumor cells themselves are also known to provide for their increased energy consumption by producing lactate (Warburg effect). The increased levels of lactate found within the tumor stroma in our study can thus be explained by invading cancer cells or CAFs. In addition, we found in our study an upregulation of fatty acids and phospholipids in the intratumoral stroma. This may be explained by the increased cellularity of the tumor-associated stroma due to immune response and inflammation, as well as malignant cell invasion. Fatty acids and lipids showed similar fold changes to those observed in the tumor tissue itself, which may be an indication that these signals are mainly from invading tumor cells.

Associations of metabolomic profiles with clinical factors

Our findings were consistent with a high-performance liquid chromatography-electrospray ionization-mass spectrometry (HPLC-ESI-MS) study of 257 breast cancer samples and 10 control samples (30). Seven of the 11 lipids that we found to be upregulated in cancer tissue were also found by the HPLC-ESI-MS study. Furthermore, these lipids showed the same association to tumor grade and HR status in terms of relative

Downloaded from http://aacrjournals.org/cancerres/article-pdf/75/9/1828/2729351/1828.pdf by guest on 21 February 2024

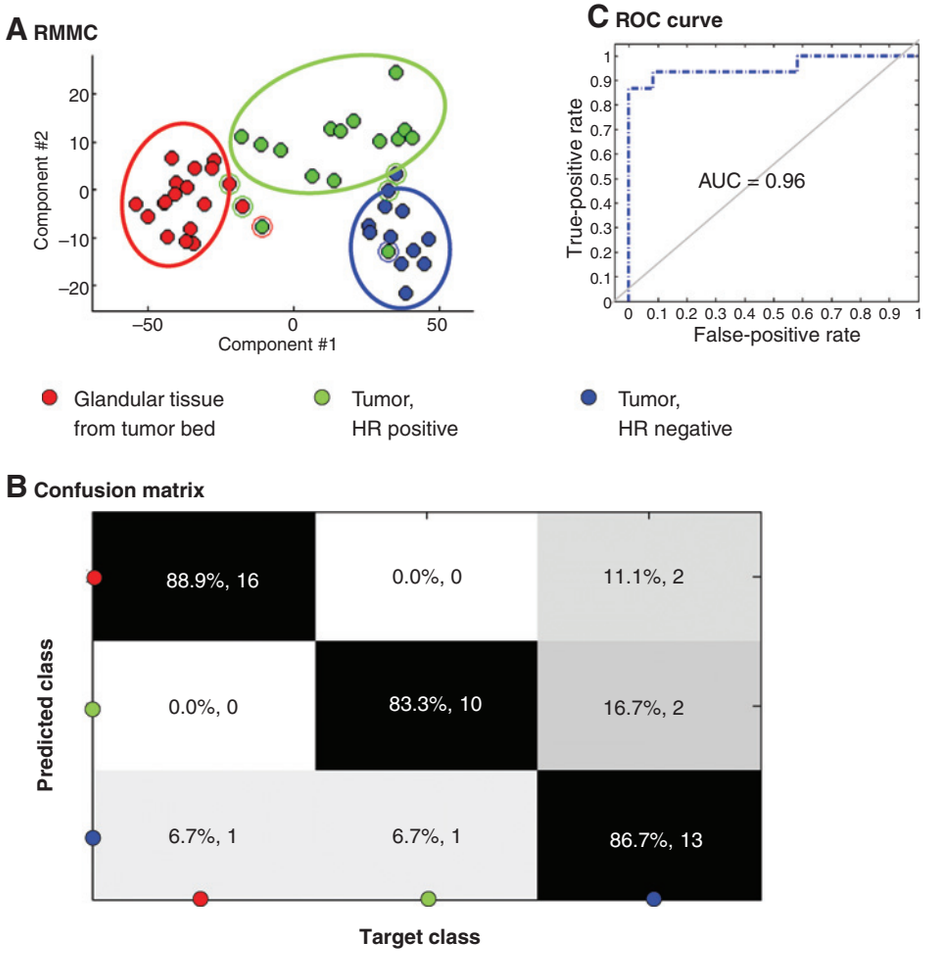

Figure 4.
Association of metabolomic DESI MSI profiles of normal glandular and tumor tissue with hormone receptor status. A, 10-fold cross-validated RMMC score plot (each patient is maximally represented by one point in each group; for each point maximum, 100 randomly selected spectra were averaged) showing the separation of normal glandular tissue, tumors with positive HR status (ER/PR receptor positive), and tumors with negative HR status (ER/PR receptor negative) using multivariate data analysis. B, confusion matrix showing classification results based on mahalanobis distance (86.7% overall correct assignment). C, ROC curve showing the potential of the model to discriminate between positive and negative HR status.

compound concentrations in our data as described in the HPLC-ESI-MS study.

In conclusion, using DESI MSI, we were able to differentiate between tumor tissue and morphologically normal breast tissue with an overall accuracy of 98.2%. In comparison with morphologically normal glandular tissue, tumor tissue had increased levels of fatty acids and showed an increase in the concentration of the majority of measured phospholipids. These findings support the theory of *de novo* lipogenesis in tumor tissue and were associated with loss of differentiation and increased levels of tumor cell proliferation. In addition, we demonstrated changes in tumor-associated stroma that correlate with findings that tumor supporting stroma may be associated with disease prognosis by playing a role in angiogenesis and extracellular matrix remodeling. We found that tumor grade and HR status accounted for the greatest differences in the metabolic profiles of tumor tissue, with tumor type being less significant. The combination of tumor grade and HR status allowed for the differentiation of normal glandular tissue, grade 2 tumors with a positive HR status and grade 3 tumors with negative HR status with an overall accuracy of 87.7%. Therefore, DESI MSI may prove to be a useful tool in the future diagnosis of breast cancer and spatially resolved characterization of tumor-associated changes in lipid biochemistry.

Disclosure of Potential Conflicts of Interest

No potential conflicts of interest were disclosed.

Disclaimer

The research was supported by the National Institute for Health Research (NIHR) Biomedical Research Centre based at Imperial College Healthcare NHS Trust and Imperial College London. The views expressed are those of the author(s) and not necessarily those of the NHS, the NIHR, or the Department of Health.

Authors' Contributions

Conception and design: S. Guenther, L.J. Muirhead, Z. Takats
Development of methodology: N. Strittmatter, R.D. Goldin, K. Veselkov, Z. Takats
Acquisition of data (provided animals, acquired and managed patients, provided facilities, etc.): S. Guenther, L.J. Muirhead, A.V.M. Speller, N. Strittmatter, R.D. Goldin
Analysis and interpretation of data (e.g., statistical analysis, biostatistics, computational analysis): S. Guenther, A.V.M. Speller, O. Golf, E.A. Jones, K. Veselkov
Writing, review, and/or revision of the manuscript: S. Guenther, L.J. Muirhead, A.V.M. Speller, O. Golf, R.D. Goldin, K. Veselkov, A. Darzi, Z. Takats
Administrative, technical, or material support (i.e., reporting or organizing data, constructing databases): L.J. Muirhead, A.V.M. Speller, R. Ramakrishnan, R.D. Goldin, Z. Takats
Study supervision: R. Ramakrishnan, K. Veselkov, A. Darzi, Z. Takats
Other [interpretation of pathology sections (H&E) and correlation with mass spectrometric findings in all cases]: R. Ramakrishnan

Downloaded from http://aacrjournals.org/cancerres/article-pdf/75/9/1828/2729351/1828.pdf by guest on 21 February 2024

Acknowledgments

The authors would like to acknowledge the NIHR Biomedical Research Centre for funding surgical metabonomics projects at Imperial College London (London, United Kingdom). K. Veselkov acknowledges a junior research fellowship scheme for supporting this research project.

Grant Support

This work was supported by the European Research Council under the Starting Grant scheme (contract no. 210356), European Commission FP7 Intelligent Surgical Device project (contract no. 3054940), and NIHR Biomedical Research Centre (Imperial College London, London, United Kingdom).

The costs of publication of this article were defrayed in part by the payment of page charges. This article must therefore be hereby marked *advertisement* in accordance with 18 U.S.C. Section 1734 solely to indicate this fact.

Received August 5, 2014; revised January 8, 2015; accepted January 20, 2015; published OnlineFirst February 17, 2015.

References

1. Hammond MEH, Hayes DF, Dowsett M, Allred DC, Hagerty KL, Badve S, et al. American society of clinical oncology/college of american pathologists guideline recommendations for immunohistochemical testing of estrogen and progesterone receptors in breast cancer. J Clin Oncol 2010;28:2784–95.
2. Flanagan MB, Dabbs DJ, Brufsky AM, Beriwal S, Bhargava R. Histopathologic variables predict Oncotype DX (TM) Recurrence Score. Mod Pathol 2008;21:1255–61.
3. Mook S, Van't Veer LJ, Rutgers EJT, Piccart-Gebhart MJ, Cardoso F. Individualization of therapy using Mammaprint: from development to the MINDACT Trial. Cancer Genom Proteomics 2007;4:147–55.
4. Parker JS, Mullins M, Cheang MCU, Leung S, Voduc D, Vickery T, et al. Supervised Risk Predictor of Breast Cancer Based on Intrinsic Subtypes. J Clin Oncol 2009;27:1160–67.
5. Cuzick J, Dowsett M, Pineda S, Wale C, Salter J, Quinn E, et al. Prognostic value of a combined estrogen receptor, progesterone receptor, Ki-67, and human epidermal growth factor receptor 2 immunohistochemical score and comparison with the genomic health recurrence score in early breast cancer. J Clin Oncol 2011;29:4273–78.
6. Bartlett JMS, Thomas J, Ross DT, Seitz RS, Ring BZ, Beck RA, et al. Mammostrat (R) as a tool to stratify breast cancer patients at risk of recurrence during endocrine therapy. Breast Cancer Res 2010;12:R47.
7. Heaphy CM, Bisoffi M, Fordyce CA, Haaland CM, Hines WC, Joste NE, et al. Telomere DNA content and allelic imbalance demonstrate field cancerization in histologically normal tissue adjacent to breast tumors. Int J Cancer 2006;119:108–16.
8. Trujillo KA, Heaphy CM, Mai M, Vargas KM, Jones AC, Phung V, et al. Markers of fibrosis and epithelial to mesenchymal transition demonstrate field cancerization in histologically normal tissue adjacent to breast tumors. Int J Cancer 2011;129:1310–21.
9. Finak G, Bertos N, Pepin F, Sadekova S, Souleimanova M, Zhao H, et al. Stromal gene expression predicts clinical outcome in breast cancer. Nat Med 2008;14:518–27.
10. Heaphy CM, Griffith JK, Bisoffi M. Mammary field cancerization: molecular evidence and clinical importance. Breast Cancer Res Treat 2009; 118:229–39.
11. Roman-Perez E, Casbas-Hernandez P, Pirone JR, Rein J, Carey LA, Lubet RA, et al. Gene expression in extratumoral microenvironment predicts clinical outcome in breast cancer patients. Breast Cancer Res 2012;14: R51.
12. Nabavizadeh N, Klifa C, Newitt D, Lu Y, Chen Y-Y, Hsu H, et al. Topographic enhancement mapping of the cancer-associated breast stroma using breast MRI. Integr Biol 2011;3:490–96.
13. Gode D, Volmer DA. Lipid imaging by mass spectrometry - a review. Analyst 2013;138:1289–315.
14. McDonnell LA, Heeren RMA. Imaging mass spectrometry. Mass Spectrom Rev 2007;26:606–43.
15. Chaurand P. Imaging mass spectrometry of thin tissue sections: a decade of collective efforts. J Proteomics 2012;75:4883–92.
16. Seeley EH, Caprioli RM. Imaging mass spectrometry: towards clinical diagnostics. Proteomics Clin Appl 2008;2:1435–43.
17. Seeley EH, Caprioli RM. MALDI imaging mass spectrometry of human tissue: method challenges and clinical perspectives. Trends Biotechnol 2011;29:136–43.
18. Schoene C, Hoefler H, Walch A. MALDI imaging mass spectrometry in cancer research: Combining proteomic profiling and histological evaluation. Clin Biochem 2013;46:539–45.
19. Dill AL, Ifa DR, Manicke NE, Zheng O, Cooks RG. Mass spectrometric imaging of lipids using desorption electrospray ionization. J Chromatogr B Analyt Technol Biomed Life Sci 2009;877:2883–89.
20. Eberlin LS, Ferreira CR, Dill AL, Ifa DR, Cooks RG. Desorption electrospray ionization mass spectrometry for lipid characterization and biological tissue imaging. Biochimica Et Biophysica Acta-Molecular and Cell Biology of Lipids 2011;1811:946–60.
21. Eberlin LS, Norton I, Orringer D, Dunn IF, Liu X, Ide JL, et al. Ambient mass spectrometry for the intraoperative molecular diagnosis of human brain tumors. Proc Natl Acad Sci 2013;110:1611–16.
22. Santagata S, Eberlin LS, Norton I, Calligaris D, Feldman DR, Ide JL, et al. Intraoperative mass spectrometry mapping of an onco-metabolite to guide brain tumor surgery. Proc Natl Acad Sci USA 2014;111:11121–26.
23. Calligaris D, Caragacianu D, Liu X, Norton I, Thompson CJ, Richardson AL, et al. Application of desorption electrospray ionization mass spectrometry imaging in breast cancer margin analysis. Proc Natl Acad Sci 2014;111: 15184–89.
24. Schramm T, Hester A, Klinkert I, Both JP, Heeren RMA, Brunelle A, et al. imzML—A common data format for the flexible exchange and processing of mass spectrometry imaging data. J Proteomics 2012;75:5106–10.
25. Alexandrov T. MALDI imaging mass spectrometry: statistical data analysis and current computational challenges. Bmc Bioinformatics 2012; 13:S11.
26. Veselkov KA, Mirnezami R, Strittmatter N, Goldin RD, Kinross J, Speller AVM, et al. Chemo-informatic strategy for imaging mass spectrometry-based hyperspectral profiling of lipid signatures in colorectal cancer. Proc Natl Acad Sci USA 2014;111:1216–21.
27. Smith CA, O'Maille G, Want EJ, Qin C, Trauger SA, Brandon TR, et al. METLIN - A metabolite mass spectral database. Ther Drug Monit 2005;27: 747–51.
28. Schmelzer K, Fahy E, Subramaniam S, Dennis EA. The lipid maps initiative in lipidomics. Lipidomics and Bioactive Lipids: Mass-Spectrometry-Based Lipid Analysis 2007;432:171–83.
29. Wishart DS, Jewison T, Guo AC, Wilson M, Knox C, Liu Y, et al. HMDB 3.0-the human metabolome database in 2013. Nucleic Acids Res 2013;41: D801–D07.
30. Hilvo M, Denkert C, Lehtinen L, Mueller B, Brockmoeller S, Seppanen-Laakso T, et al. Novel theranostic opportunities offered by characterization of altered membrane lipid metabolism in breast cancer progression. Cancer Res 2011;71:3236–45.
31. Sakai K, Okuyama H, Yura J, Takeyama H, Shinagawa N, Tsuruga N, et al. Composition and turnover of phospholipids and neutral lipids in human breast-cancer and reference tissues. Carcinogenesis 1992;13: 579–84.
32. Hvidberg E, Langgard H, Jensenholm J. Sodium, potassium and chloride in connective tissue. Acta Pharmacologica Et Toxicologica 1963;20:131–9.
33. Dunnwald LK, Rossing MA, Li CI. Hormone receptor status, tumor characteristics, and prognosis: a prospective cohort of breast cancer patients. Breast Cancer Res 2007;9:R6.
34. Beckonert O, Monnerjahn K, Bonk U, Leibfritz D. Visualizing metabolic changes in breast-cancer tissue using H-1-NMR spectroscopy and self-organizing maps. Nmr in Biomedicine 2003;16:1–11.
35. Curtis C, Shah SP, Chin S-F, Turashvili G, Rueda OM, Dunning MJ, et al. The genomic and transcriptomic architecture of 2,000 breast tumours reveals novel subgroups. Nature 2012;486:346–52.
36. Gray J, Druker B. Genomics - The breast cancer landscape. Nature 2012;486:328–29.

Downloaded from http://aacrjournals.org/cancerres/article-pdf/75/9/1828/2729351/1828.pdf by guest on 21 February 2024

37. Goncalves A, Bertucci F. Clinical Application of Proteomics in Breast Cancer: State of the Art and Perspectives. Med Princ Pract 2011;20:4–18.
38. Geiger T, Madden SF, Gallagher WM, Cox J, Mann M. Proteomic Portrait of Human Breast Cancer Progression Identifies Novel Prognostic Markers. Cancer Res 2012;72:2428–39.
39. Claudino WM, Quattrone A, Biganzoli L, Pestrin M, Bertini I, Di Leo A. Metabolomics: Available results, current research projects in breast cancer, and future applications. J Clin Oncol 2007;25:2840–46.
40. Denkert C, Bucher E, Hilvo M, Salek R, Oresic M, Griffin J, et al. Metabolomics of human breast cancer: new approaches for tumor typing and biomarker discovery. Genome Med 2012;4:37.
41. Gatenby RA, Gillies RJ. Why do cancers have high aerobic glycolysis? Nat Rev Cancer 2004;4:891–99.
42. Sampaio JL, Gerl MJ, Klose C, Ejsing CS, Beug H, Simons K, et al. Membrane lipidome of an epithelial cell line. Proc Natl Acad Sci USA 2011;108:1903–07.
43. Punnonen K, Hietanen E, Auvinen O, Punnonen R. Phospholipids and fatty-acids in breast-cancer tissue. J Cancer Res Clin Oncol 1989;115:575–78.
44. Byun JS, Gardner K. Wounds That Will Not Heal Pervasive Cellular Reprogramming in Cancer. Am J Pathol 2013;182:1055–64.
45. Coussens LM, Werb Z. Inflammation and cancer. Nature 2002;420: 860–67.
46. Conklin MW, Keely PJ. Why the stroma matters in breast cancer Insights into breast cancer patient outcomes through the examination of stromal biomarkers. Cell Adh Migr 2012;6:249–60.
47. Cirri P, Chiarugi P. Cancer-associated-fibroblasts and tumour cells: a diabolic liaison driving cancer progression. Cancer Metastasis Rev 2012;31:195–208.
48. Pavlides S, Whitaker-Menezes D, Castello-Cros R, Flomenberg N, Witkiewicz AK, Frank PG, et al. The reverse Warburg effect Aerobic glycolysis in cancer associated fibroblasts and the tumor stroma. Cell Cycle 2009; 8:3984–4001.

Downloaded from http://aacrjournals.org/cancerres/article-pdf/75/9/1828/2729351/1828.pdf by guest on 21 February 2024